

# RSC Advances



This is an *Accepted Manuscript*, which has been through the Royal Society of Chemistry peer review process and has been accepted for publication.

*Accepted Manuscripts* are published online shortly after acceptance, before technical editing, formatting and proof reading. Using this free service, authors can make their results available to the community, in citable form, before we publish the edited article. This *Accepted Manuscript* will be replaced by the edited, formatted and paginated article as soon as this is available.

You can find more information about *Accepted Manuscripts* in the [Information for Authors](#).

Please note that technical editing may introduce minor changes to the text and/or graphics, which may alter content. The journal's standard [Terms & Conditions](#) and the [Ethical guidelines](#) still apply. In no event shall the Royal Society of Chemistry be held responsible for any errors or omissions in this *Accepted Manuscript* or any consequences arising from the use of any information it contains.

## Corrosion behaviour of Tetrahedral Amorphous Carbon (ta-C) filled Titania Nano Tubes

L. Mohan <sup>a, b</sup>, S. Viswanathan <sup>a</sup>, C. Anandan <sup>a, \*</sup> N. Rajendran <sup>b, \*</sup>

<sup>a</sup> *Surface Engineering Division, CSIR-National Aerospace Laboratories  
P.O.Box:1779, Old Airport Road, Bangalore, Karnataka, India*

<sup>b</sup> *Department of Chemistry, Anna University, Chennai, Tamilnadu, India*

### Abstract

TiO<sub>2</sub> nanotubes were formed by anodic oxidation on Ti-6Al-7Nb and the nanotubes were filled with tetrahedral amorphous carbon (ta-C) by cathodic arc evaporation (CAE). The samples were characterized by field emission scanning electron microscopy (FESEM), energy dispersive spectroscopy (EDS) and micro Raman studies. The corrosion behaviour of the Ti-6Al-7Nb substrate, substrate with self-organized TiO<sub>2</sub> nanotubes (TNT) and ta-C filled TiO<sub>2</sub> nano tubes (ta-C TNT) were investigated through electrochemical impedance spectroscopy (EIS) and potentiodynamic polarization studies in simulated body fluid (Hanks' solution). The investigations show that the native oxide on the sample is replaced by a self assembled nano array by an anodisation process and the pores can be filled with ta-C. Potentiodynamic polarization and electrochemical impedance studies of ta-C filled TNT sample show that the corrosion resistance is comparable with TNT samples.

**Keywords:** anodic oxidation, nanotubes, ta-C, pore filling, corrosion, EIS

\*Corresponding authors E-mail addresses: [canandan@nal.res.in](mailto:canandan@nal.res.in) (C. Anandan),  
[nrajendran@annauniv.edu](mailto:nrajendran@annauniv.edu) (N. Rajendran).

## 1. Introduction

Owing to their exceptional mechanical, chemical and biological properties titanium and its alloys are extensively used in medicine as materials for artificial dental or hip Implants.<sup>1-4</sup> Although titanium alloys possess high strength-to-weight ratio and good corrosion resistance, they suffer from poor wear resistance.<sup>5,6</sup> The high degree of biocompatibility of Ti and its alloys is attributed to their capability to form stable and dense oxide layers, usually 2–5 nm thick, consisting principally of TiO<sub>2</sub>. Whenever Ti is mechanically damaged the native oxide layer is spontaneously rebuilt in most environments. By electrochemical anodization in various solutions, thicker oxide layers can be grown on the alloys. Anodization of titanium and its alloys has been examined by many groups, and the mechanisms leading oxide formation and growth are well established.<sup>7-12</sup> High aspect ratio self-organized oxide nanotube structures have been reported, via controlling the composition of aqueous and organic electrolytes.<sup>13-15</sup> In addition, ordered oxide nanotube layers on Ti–Nb,<sup>16</sup> Ti–Zr,<sup>17</sup> Ti–Nb–Ta–Zr,<sup>18</sup> Ti–Al–V,<sup>19, 20</sup> and Ti–Al–Nb<sup>21</sup> alloys have also been reported.

The immense flexibility of carbon materials come up from the strong dependence of their properties on the ratio of sp<sup>2</sup> (graphite-like) to sp<sup>3</sup> (diamond-like) bonds in the material. A high fraction of sp<sup>3</sup> bonds in an amorphous carbon leads to high hardness while lower fraction leads to softer material. Generally, an amorphous carbon can have any mixture of sp<sup>3</sup>, sp<sup>2</sup> and even sp<sup>1</sup> sites, with the potential presence of up to 60 at. % hydrogen.<sup>22-24</sup> The hydrogenated amorphous carbons (a-C:H) have a relatively small C–C sp<sup>3</sup> content. DLCs with higher sp<sup>3</sup> contents are termed as tetrahedral amorphous carbon (ta-C) and their hydrogenated analogue, ta-C:H.<sup>25</sup> Tetrahedral amorphous carbon (ta-C) is extensively used as a coating because of its properties

comparable to diamond, such as high hardness, chemical inertness, superior wear resistance and low coefficient of friction.<sup>26</sup> It has been demonstrated that the exceptional mechanical behavior of ta-C film is mostly determined by its high percentage of sp<sup>3</sup> hybridization.<sup>27</sup> These properties make it ultimate for wear resistance on cutting tools, automotive components, aerospace components and biomedical applications.

The purpose of the present study is to fill tetrahedral amorphous carbon (ta-C) into nanotubes formed on Ti-6Al-7Nb alloy by anodisation followed by cathodic arc evaporation and characterize them for their nanoscale features, corrosion behaviour by electrochemical impedance spectroscopy (EIS) and potentiodynamic polarization studies in simulated body fluid (Hanks' solution).

## **2. Materials and methods**

### ***2.1 Preparation of the samples***

Titanium alloy, Ti-6Al-7Nb (ASTM F1295 grade) was procured from TIMET, USA in the form of one inch diameter rod. Test samples of about ~3 mm thickness, cut from the rod were ground with different grades of silicon carbide papers and finally polished using 0.1 µm diamond paste. These samples were ultrasonically cleaned using acetone and dried. A two electrode electrochemical anodisation cell, with platinum as cathode and the Ti-6Al-7Nb substrate as anode, was used to fabricate the nanotube arrays. Anodisation was carried out in an electrolyte consisting HF and sulfuric acid at 30 V with a DC power supply for 1 h.<sup>28</sup> After anodization, the nano tubes were filled with tetrahedral amorphous carbon (ta-C) coating using cathodic arc evaporation (CAE) with graphite as target and argon as working gas in a vacuum chamber made up of stainless steel (304). The chamber was pumped to  $2.4 \times 10^{-6}$  milliBar pressure by turbo

molecular pump backed with a rotary pump. Argon flow (10 sccm) was controlled by MKS make mass flow controllers. The desired processing pressure (5  $\mu$ bar) in the deposition chamber was controlled by a throttle valve at the specified flow rate of the gas and ta-C filling was carried out for 0.5, 1, 2, 5 and 10 minutes. The substrates were biased with negative DC voltage (-110 V) using DC power supply.

## 2.2. Electrochemical measurements

Electrochemical studies on the Ti6Al-7Nb substrate, TNT and ta-C filled TNT (10 min) samples were conducted using CH 604D Electrochemical Workstation supplied by CH instruments, USA. The conventional three electrode glass cell was used to carry out the electrochemical studies. The tests were conducted in 200 ml of Hanks' solution which simulates the body fluid (SBF) at room temperature. The sample was kept as the working electrode (1  $\text{cm}^2$ ); Pt foil and saturated calomel electrode (SCE) were used as counter and reference electrodes, respectively. The reference electrode was kept very close to the surface of the working electrode. The sample was immersed in Hanks' solution for an hour in order to establish the open circuit potential ( $E_{\text{OCP}}$ ) or the steady state potential. EIS measurement was carried out in the frequency range of 10 mHz to 100 kHz. The applied alternating sinusoidal potential was 10 mV on the  $E_{\text{OCP}}$ . After each experiment, the impedance data were displayed as Bode plots. The Bode plot is a plot of  $\log |Z|$  vs.  $\log f$  and  $\log f$  vs. - phase angle ( $\theta$ ), where  $|Z|$  is the absolute impedance and  $f$  is the frequency. The acquired data were curve fitted and analyzed using ZSimpwin program (Princeton Applied Research, USA) to get suitable equivalent circuit parameters. The quality of the fit was checked by the  $\chi^2$  value. After EIS measurements,

potentiodynamic polarization studies were carried out in a potential range below 200 mV and above the OCP value with a scan rate of 1 mV/s. The Tafel plot was obtained after the electrochemical measurements have been represented in the form of potential vs.  $\log(i)$  plot. The corrosion potential ( $E_{\text{corr}}$ ) and corrosion current ( $I_{\text{corr}}$ ) were deduced from the Tafel plot.<sup>29-31</sup>

### ***2.3. Characterization techniques***

The surface morphology of the samples were examined by Carl Zeiss Supra 40 VP FESEM equipped Inca Penta Fctx3 (Oxford Instruments) EDS analyzer for elemental analysis. The 2D and 3D profiles of FESEM images were obtained by using the scanning probe image processor WSxM 5.0 develop 7.0 software.<sup>32</sup> Water Contact Angle (CA) of the samples was measured using Surface Electro Optics Phoenix contact angle meter (South Korea) by sessile drop method. Water droplets of about 8•0  $\mu\text{L}$  were carefully dropped onto the samples through a syringe, and the CAs were obtained by measuring at different positions on each sample and the average value is reported. Micro Raman studies were performed with DILOR-JOBIN-SPEX made LABRAM 010, France. A He–Ne laser source having a wavelength of 632 nm was used.

### 3. Results and discussion

**Fig. 1 (a)** shows the FESEM image of an anodic TiO<sub>2</sub> nano tube array (TNT) obtained after anodisation of Ti-6Al-7Nb for 1h at 30 V. In these images, the high degree of ordering of the tubes can be clearly seen. FESEM images of the TNT show that the arrays have very regular and vertically aligned tube structure. **Fig. 1 (b-f)** shows the FESEM images of TNT filled with tetrahedral amorphous carbon (ta-C) for 0.5, 1, 2, 5 and 10 min, respectively. (EDS shown in Supplementary (S-1)). As can be seen from the **Fig.1 (b)**, in 0.5 min, filling of ta-C takes place in inter-tubular space and pores. After 1 min, ta-C filled into inter-tubular space and pores formed network like growth of carbon can be seen from **Fig.1 (c)**. In **Fig.1 (d)**, 2 min filling, shows nodular like structure. Similarly, after 5 min in **Fig.1 (e)**, uniform spherical shape morphology can be seen which has covered the tubular pores and porous space. Further increase in deposition time to 10 min, the formed spherical morphology fuse together and completely cover the TNT which can be seen in **Fig.1 (f)**.(FESEM cross sectional images of TNT and 10 min ta-C filled TNT samples are shown in Supplementary (S-2)).

**Figs. 2 (a - f)** show the 2D image of the TNT and ta-C filled TNT obtained from FESEM images **Figs.1a to f**, respectively. The roughness (RMS) values obtained from 2D profiles are given in **Table 1** for the same. The roughness of the substrate after polishing is ~12 nm. As indicated in **Fig. 2 (a)** in TNT sample, the nano tubes have diameters of approximately 100 nm and an average inter-tube distance of approximately 30 nm. The height of the nanotubes is about 260 nm. **Figs. 2 (b - f)** show the 2D profiles of ta-C filled TNT after 0.5, 1, 2, 5 and 10 min, respectively. From the figures it can be clearly seen that the gradual filling of the TNT by ta-C is taking place with increasing deposition time. The roughness values decrease due to increase in

the filling time resulting in smoother layer. Further, the filling rate of nanotubes by ta-C is given in section below.

To demonstrate the filling rate of nanotubes 3D and 2D analyses were carried out on TNT and ta-C filled TNT samples. **Fig.3 (a-f)** show the 3D images obtained from FESEM images for single nanotube of TNT and ta-C filled TNT samples at 0.5, 1, 2, 5 and 10 min, respectively. Similarly, 2D profiles for the same are given in **Fig.4 (a-f)**. The change in the nanotube height and diameter after various filling times are given in **Table 1** and **Fig.5**. **Figs.3 (a)** and **4 (a)**, show single nanotube with tube height and diameter of 260 and 100 nm, respectively. After ta-C filling at various time, **Figs. 3** and **4 (b-f)**, the height and diameter of the nanotube decreases. **Table 1** and **Fig.5** present the progressive filling of ta-C in to nanotube. The wt% of carbon obtained by EDS, given in **Fig. 5** for ta-C filled TNT for 0.5, 1, 2, 5 and 10 min, shows that there is an increase in carbon content by increase of filling time indicating the filling of TNT by ta-C. These results support the earlier conclusion from FESEM images and 2D profiles that increasing the filling time increases the amount of carbon on the TNT surface.

In order to investigate the wettability of the samples, water contact angle was measured and the collected results are shown in **Table. 1** and **Fig.5**. On as-prepared TNT wetting by water was observed but after filling the TNT with ta-C for 0.5, 1, 2, 5 and 10 min the water contact angle is 80.5, 87, 118.8, 121.4 and 131.5 ° ±2, respectively. The transition to hydrophobic nature takes place within 2 min of deposition. The increase in contact angle towards hydrophobic nature with increase in filling time is due to the fact that carbon coatings are generally hydrophobic in nature.<sup>33</sup> This is despite the fact that surface roughness decreases with filling of TNT.

**Figs. 6(a-e)** show the Raman spectra in the 1100–1800  $\text{cm}^{-1}$  wave number range of the ta-C filled TNT samples for 0.5, 1, 2, 5 and 10 min, respectively. Raman peaks corresponding to carbon, centered around 1560  $\text{cm}^{-1}$  (G-peak) and 1360  $\text{cm}^{-1}$  (D-peak),<sup>34,35</sup> can be seen in **Fig. 4**. In the case of 0.5 min filling, **Fig.6 (a)** the D band intensity is low compared to that of 1 and 2 min samples (c and d). With increase in the deposition time, the D band intensity increases. Inset in figure. **Fig.6** shows that after 10 min of ta-C deposition intensities of D and G band are comparable.

Potentiodynamic polarization curves of the Ti-6Al-7Nb substrate, TNT, and ta-C filled TNT at 10 min samples in Hanks' solution are shown in **Fig. 7 (a-c)**, respectively. The corrosion current ( $I_{\text{corr}}$ ) was obtained by extrapolation of the cathodic and anodic branches of the polarization curves to the corrosion potential. **Table 2** shows the corrosion current density and corrosion potential for the substrate, TNT and 10 min ta-C filled TNT samples. The  $E_{\text{corr}}$  value shifted to much nobler values for TNT and ta-C filled TNT samples -0.236 and -0.202 V respectively, compared to that of substrate value of -0.303 V indicating the passive nature of the TNT and ta-C filled TNT samples in Hanks' solution. The corrosion current density of the TNT sample ( $0.038 \mu\text{A}/\text{cm}^2$ ) (**Fig.7 (b)**) shows that anodisation has increased the corrosion current density by nearly an order of magnitude. However, owing to the nano tubular morphology of the TNT covered surface the surface area of TNT sample is much higher as compared to substrate. The increased corrosion current could be due to this increased surface area and therefore, the actual corrosion resistance could be very high. The corrosion current density of the ta-C filled TNT is  $0.036 \mu\text{A}/\text{cm}^2$ . It can be also observed from **Fig. 7** that there is no clear passive region in case of TNT samples while for the ta-C filled case a passive region can be observed. Also, in this case in

the anodic region, passivation current is nearly constant compared to substrate and TNT samples and lower than the TNT which exemplifies that the stability of the passive nature of ta-C coating. The constant passivation current of the ta-C filled TNT samples implies that the TNTs are now completely covered by ta-C, and is due to the inert nature of the carbon (**Fig.7 (c)**).

The results of electrochemical impedance tests in Hanks' solution for Ti-6Al-7Nb substrate, TNT and ta-C filled TNT samples are presented in the form of Nyquist and Bode plots in **Figs. 8 (a, b, and c)**. The Nyquist plots in **Fig. 8(a)** are semicircular with the substrate and having a larger diameter compared to that of TNT and ta-C filled TNT. In **Fig. 8 (b)**, for substrate, the phase angle changes rapidly from  $-6^\circ$  to  $-20^\circ$  in the high frequency range (10 kHz to 100 kHz). In the low frequency range from 0.01 to 100 Hz, the phase angle remains nearly constant for substrate  $-82.5^\circ$ , which is less than the value for an ideal capacitor ( $-90^\circ$ ). In the same frequency range, a linear relationship between  $\log |z|$  and  $\log f$  is observed with a slope close to one. In the case of TNT, there is an inflexion point in the phase angle in the frequency range of 1 to 10 Hz. In the case of ta-C filled TNT, the phase angle changes rapidly from  $-2^\circ$  to  $-20^\circ$  in the high frequency range (10 to 100 kHz), as the frequency is reduced from 100 to 10 Hz, there is a steady increase of the phase angle in this frequency range from  $-2$  to  $70^\circ$ . In lower frequency, there is another inflexion point in the phase angle in the frequency range of 10 to 0.01 Hz.

**Fig. 9 (a-c)** shows the equivalent circuit model with schematic representation used for fitting the EIS data of the substrate, TNT and ta-C filled TNT samples, respectively. **Fig. 9 (a)**, for substrate, the equivalent electrochemical circuit is composed of resistances and constant phase elements (CPE). The resistive components  $R_e$ ,  $R_1$  and  $R_2$  are related to the solution resistance,

resistance of the outer porous layer and inner layer resistance, respectively. The Q symbol signifies the possibility of a non-ideal capacitance, known as constant phase element (CPE), and its impedance is defined as  $Z_{CPE} = [Q(j\omega^n)]^{-1}$  with 'n' less than 1; for an ideal capacitance  $n = 1$ . In this, Q1 represents the capacitance of the outer layer, Q2 the capacitance of the inner layer. Similar equivalent circuits have also been proposed for titanium alloys in Hanks' solutions by previous researchers.<sup>36-38</sup> The values of the electrical parameters obtained by fitting the impedance data of the substrate is given in **Table 3**. The quality of the fitting to equivalent circuit was qualified by  $\chi^2$  value and the error distribution versus the frequency comparing experimental with simulated data. For the substrate, the high corrosion resistance R2 is associated with inner layer on the substrate, which is  $5.4 \times 10^6 \Omega\text{cm}^2$  in the present case. The Q2 component is associated to the capacitance of this inner barrier layer. The resistance of outer porous layer is  $21.5 \Omega\text{cm}^2$ . The value "n" for the constant phase element representing the inner layer is 0.98 and that representing the outer layer is 0.92.

In the case of TNT samples, the equivalent circuit has three time constants and EC is given in **Fig. 9 (b)**. For TNT samples, the outer porous oxide layer of the substrate is replaced by the inter-tube space and pores. In this, Q1 and R1 represent the capacitance and resistance of the inter-tubular space respectively. The elements comprising Q2 and R2 and Q3 and R3 are associated with the capacitance and resistance of the nano tubes. The fitting parameters for TNT sample in **Table 3** shows that the resistance R1 of the layer which is in direct contact to substrate oxide via inter tubular space is about  $1.5 \times 10^4 \Omega\text{cm}^2$ . The resistance R3 is associated with the nano tubes ( $1.5 \times 10^6 \Omega\text{cm}^2$ ). The non ideal value for the constant phase element representing the Q1, Q2 and Q3 is 0.92 0.91 and 0.92, respectively. The resistance of the nanotubes are in the order of  $R2 < R1 < R3$ . The high corrosion resistance of the TNT is

combination of R1 and R3 which is associated with substrate oxide (inter tubular space) and of the tubes.<sup>39-41</sup>

In the case of ta-C filled TNT samples **Fig. 9(c)**, Q1 and R1 represents the capacitance and resistance of the ta-C layer, which has completely filled and covered the TNTs. The fitting parameters in **Table 3** in this case show that the resistance R1 of the outer layer is  $2.3 \times 10^5 \Omega \text{cm}^2$ . The Q2 and R2 correspond to the capacitance and resistance which could be due to the pores and/or pin holes in the ta-C layer, respectively. The value of R2 is  $82 \Omega \text{cm}^2$ . The constant phase element, Q3 and resistance R3 are associated with the inner barrier layer at the bottom of nanotubes closer to the substrate. The non ideal value for the constant phase elements representing the Q1, Q2 and Q3 is 0.90, 0.82 and 0.90, respectively. The corrosion resistance of various elements in the equivalent circuit are in the order  $R1 > R3 > R2$ . The high corrosion resistance R1 is associated with the ta-C filling the TNT. The resistance R3,  $1.3 \times 10^4 \Omega \text{cm}^2$ , is due to  $\text{TiO}_2$  at the bottom of nanotubes closer to the substrate. The above results show that the corrosion resistance of TNT samples is lower compared to that of pure substrate and this could be explained by the fact that nanostructures have more surface area compared to flat substrates. The corrosion resistance of ta-C filled TNT samples is comparable to TNT samples. In addition to the above, it is well known that the ta-C depositions on titanium alloys improve their tribological properties and nanostructured surfaces improve the adhesion of coatings to the substrate. It should be mentioned here that TNT was required for obtaining a strongly adherent ta-C coating on the substrate otherwise the coating peeled off. Therefore, filling of nanotubes with ta-C can be a promising method for surface modification of titanium alloys to enhance their mechanical properties.

## Conclusions

Self-organized titanium oxide nanotube arrays with pore diameters 100 nm were formed on titanium alloy Ti-6Al-7Nb by anodic oxidation. The nano tubes were filled with tetrahedral amorphous carbon (ta-C) by cathodic arc deposition for various times. The 2D, 3D and EDS analyses confirm the gradual filling of ta-C into nanotubes. Potentiodynamic polarization and electrochemical impedance studies of ta-C filled TNT sample in Hanks' solution show that the corrosion resistance of ta-C filled TNT samples is comparable with TNT samples.

## Acknowledgments

The work was carried out under the CSIR network project on ESC-01-03. The authors would like to thank the Director, National Aerospace Laboratories, Bangalore for his support and permission to publish the work. The authors would like to thank Dr. Harish C. Barshilia for providing the Cathodic Arc source, Mr. Jakheer Khan, Mr. Shanthi Swaroop for arc deposition, Mr. Siju and Mr. N.T. Manikandanath, SED, NAL for FESEM and micro Raman studies.

## References

- [1] Liu X, Chu PK, Ding C, *Mater. Sci, Eng. R.* 2004, **47**, 49.
- [2] Geetha M, Singh AK, Asokamani R, Gogia AK, *Prog. Mater. Sci.*, 2009, **54**, 397.
- [3] Variola F, Brunski JB, Orsini G, Paulo Tambasco de Oliveira, Wazen R, Nanci A, *Nanoscale*, 2011,**3**, 335.
- [4] Mohan L, Durgalakshmi D, Geetha M, Sankaranarayanan TSN, Asokamani R, *Ceram. Inter.* 2012, **38(4)**, 3435.
- [5] Mohan L, Anandan C, *Appl. Surf. Sci.* 2013, **282**, 281.
- [6] Anandan C, Dilli Babu P, Mohan L, *J. Mater. Eng. Perform*, 2013, **22(9)**, 2623.
- [7] Feng XJ, Macak JM, Albu SP, Schmuki P, *Acta Biomater.*, 2008, **4**, 318.
- [8] Yang BC, Uchida M, Kim HM, Zhang XD, Kokubo T, *Biomater.*, 2004,**25**,1003.
- [9] Taveira LV, Macak JM, Tsuchiya H, Dick LFP, Schmuki P, *J. Electrochem. Soc.*, 2005,**152**, B405.
- [10] Macak JM, Tsuchiya H, Schmuki P, *Angew Chem, Int. Ed.*, 2005,**44**,2100.
- [11] Regonini D, Bowen CR, Jaroenworoluck A, Stevens R, *Mater. Sci. Engn. R*, 2013, **74**, 377.
- [12] Regonini D, Satka A, Jaroenworoluck A, Allsopp DWE, Bowen CR, Stevens R, *Electrochimica Acta*, 2012, **74**, 244.
- [13] Gong D, Grimes CA, Varghese OK, Chen Z, Dickey EC, *J. Mater. Res.*, 2001, **16**, 3331.
- [14] Beranek R, Hildebrand H, Schmuki P, *Electrochem. Solid State Lett.*, 2003,**6**, B12.
- [15] Macak JM, Tsuchiya H, Taveira L, Aldabergerova S, Schmuki P, *Angew. Chem. Int. Ed.*, 2005;**44**,7473.
- [16] Ghicov A, Aldabergerova S, Tsuchyia H, Schmuki P, *Angew. Chem., Int. Ed.*, 2006,**45**, 6993.

- [17] Yasuda K, Schmuki P, *Adv. Mater.*, 2007, **19**, 1757.
- [18] Tsuchiya H, Macak JM, Ghicov A, Schmuki P, *Small*, 2006, **2**, 888.
- [19] Mohan L, Anandan C, Rajendran N, *Electrochimica Acta*, 2015, **155**, 411.
- [20] Matykina E, Hernandez-Lopez JM, Conde A, Domingo C, de Damborenea JJ, Arenas MA, *Electrochimica Acta*, 2011, **56**, 2221.
- [21] Mohan L, Anandan C, Rajendran N, *Mater. Sci. Eng. C*, 2015, **50**, 394.
- [22] Robertson J, *Prog. Solid State Chem.*, 1991, **21**, 199.
- [23] Robertson J, *Adv. Phys.* 1986, **35**, 317.
- [24] Robertson J, *Pure Appl. Chem.* 1994, **66**, 1789.
- [25] Teo KBK, Ferrari AC, Fanchini G, Rodil SE, Yuan J, Tsai JTH, Laurenti E, Tagliaferro A, Robertson J, Milne WI, *Diamond Relat. Mater.* 2002, **11**, 1086.
- [26] Wei Q, Narayan J, *Int. Mater. Rev.*, 2000, **45**, 135.
- [27] Robertson J, *Mater. Sci. Eng., R*, 2002, **37**, 129.
- [28] Mohan L, Anandan C, Rajendran N, *RSC Adv.*, 2015, **5**, 41763
- [29] Mohan L, Dilli Babu P, Kumar P, Anandan C, *Surf. Interf. Anal.* 2013, **45**, 1785.
- [30] Anandan C, Mohan L. *J. Mater. Eng. Perform.* 2013, **22**, 3507.
- [31] Prateek Kumar, Dilli Babu P, Mohan L, Anandan C, Grips VKW, *J. Mater. Eng. Perform.* 2013, **22**, 283.
- [32] Horcas I, Fernandez R, Gomez-Rodriguez JM, Colchero J, Gómez-Herrero JWSXM, Baro AM. *Rev. Sci. Instrum.* 2007, **78**, 013705.
- [33] Zhang C, Fujii M, *J. Surf. Eng. Mater. Adv. Technol.*, 2015, **5**, 110.
- [34] Mohan L, Anandan C, Grips VKW, *Appl. Surf. Sci.* 2012, **258**, 6331.
- [35] Anandan C, Mohan L, Dilli Babu P, *Appl. Surf. Sci.* 2014, **296**, 86.

- [36] Mohan L, Anandan C, Grips VKW, *J. Mater. Sci. Mater. Med.* 2013, **24**, 623.
- [37] Mohan L, Anandan C, *Appl. Surf. Sci.* 2013, **268**, 288.
- [38] S. Tamilselvi, V. Raman and N. Rajendran, *Electrochim. Acta*, 2006, 52, 839.
- [39] Muñoz AG, Chen Q, Schmuki P, *J. Solid State Electrochem.*, 2007, **11**, 1077.
- [40] Wu G, Yu M, Liu J, Li S, Wu L, Zhang Y, *Surf. Interf. Anal.* 2013, **45**, 661.
- [41] Oyarzún DP, Córdova R, Pérez OEL, Muñoz E, Henríquez R, Teijelo M L, Gómez H, J *Solid State Electrochem*, 2011, **15**, 2265.

### Figure Captions

**Fig. 1** FESEM images of TNT (a) and ta-C filled TNT samples at (b) 0.5 min, (c) 1 min, (d) 2 min, (e) 5 min and (f) 10 min.

**Fig. 2** 2D line profiles obtained from FESEM images (a) TNT and ta-C filled TNT samples at (b) 0.5 min, (c) 1 min, (d) 2 min, (e) 5 min and (f) 10 min.

**Fig. 3** 3D images obtained from FESEM images for single nanotube (a) TNT and ta-C filled TNT samples at (b) 0.5 min, (c) 1 min, (d) 2 min, (e) 5 min and (f) 10 min.

**Fig. 4** 2D profiles obtained from FESEM images for single nanotube (a) TNT and ta-C filled TNT samples at (b) 0.5 min, (c) 1 min, (d) 2 min, (e) 5 min and (f) 10 min.

**Fig. 5** Roughness (RMS), nanotube diameter (nm) (Left) and carbon (wt %), contact angle (deg), tube height (nm) (Right) obtained from ta-C filled TNT samples at different filling time (0.5, 1, 2, 5 and 10 min).

**Fig. 6** Raman spectra for ta-C filled TNT at (a) 0.5 min, (b) 1 min, (c) 2 min, (d) 5 min and (e) 10 min (inset at 10 min).

**Fig. 7** Potentiodynamic polarization curves for (a) Ti-6Al-7Nb substrate (b) TNT and (c) ta-C filled TNT samples.

**Fig. 8** (a) Nyquist plot, Bode plots (b) phase and (c) magnitude for substrate, TNT and ta-C filled TNT samples

**Fig. 9** Equivalent circuit (EC) diagram with schematic representation used for fitting EIS data of (a) substrate, (b) TNT (c) ta-C filled TNT samples.

## List of Tables

**Table 1:** Roughness, tube height, diameter, contact angle, and carbon wt % of TNT and ta-C filled TNT samples

S.No	Parameters	RMS (nm)	Tube height (nm)	Tube diameter (nm)	Contact angle (deg)	Carbon (wt %)
1	TNT	108.2	260	100	Wetting	-
2	0.5 min	79.2	225	80	80.5°±2	4.56
3	1 min	64.5	150	70	87.0°±2	8.01
4	2 min	59.1	100	60	118.8°±2	9.34
5	5 min	42.2	25	30	121.4°±2	13.4
6	10 min	37.8	10	15	131.5°±2	23.5

**Table 2:** Results of potentiodynamic polarization studies

S. no	Sample	$E_{\text{corr}}$ (V)	$i_{\text{corr}}$ ( $\mu\text{A}/\text{cm}^2$ )
1.	Substrate	-0.303	$0.005 \pm 0.0006$
2.	TNT	-0.236	$0.038 \pm 0.0151$
3.	ta-C filled TNT	-0.202	$0.036 \pm 0.0116$

**Table 3:** Electrochemical impedance parameters obtained by fitting equivalent circuit model for substrate, TNT and ta-C filled TNT samples

Samples	$R_e$ $\Omega$ $\text{cm}^2$	$Q_1$ $\text{S s}^n \text{cm}^{-2}$	$n_1$	$R_1$ $\Omega \text{cm}^2$	$Q_2$ $\text{S s}^n \text{cm}^{-2}$	$n_2$	$R_2$ $\Omega \text{cm}^2$	$Q_3$ $\text{S s}^n \text{cm}^{-2}$	$n_3$	$R_3$ $\Omega \text{cm}^2$	$\chi^2$
Substrate	14	$7.3 \times 10^{-8}$	0.92	21.5	$1.7 \times 10^{-5}$	0.98	$5.4 \times 10^6$	-	-	-	$5.5 \times 10^{-4}$
TNT	15	$1.6 \times 10^{-5}$	0.92	$1.5 \times 10^4$	$1.2 \times 10^{-7}$	0.91	27.5	$5.4 \times 10^{-6}$	0.92	$1.5 \times 10^6$	$2.7 \times 10^{-4}$
ta-C filled TNT	6	$4.5 \times 10^{-8}$	0.90	$2.3 \times 10^5$	$1.1 \times 10^{-3}$	0.82	82	$2.4 \times 10^{-5}$	0.90	$1.3 \times 10^4$	$3.7 \times 10^{-3}$

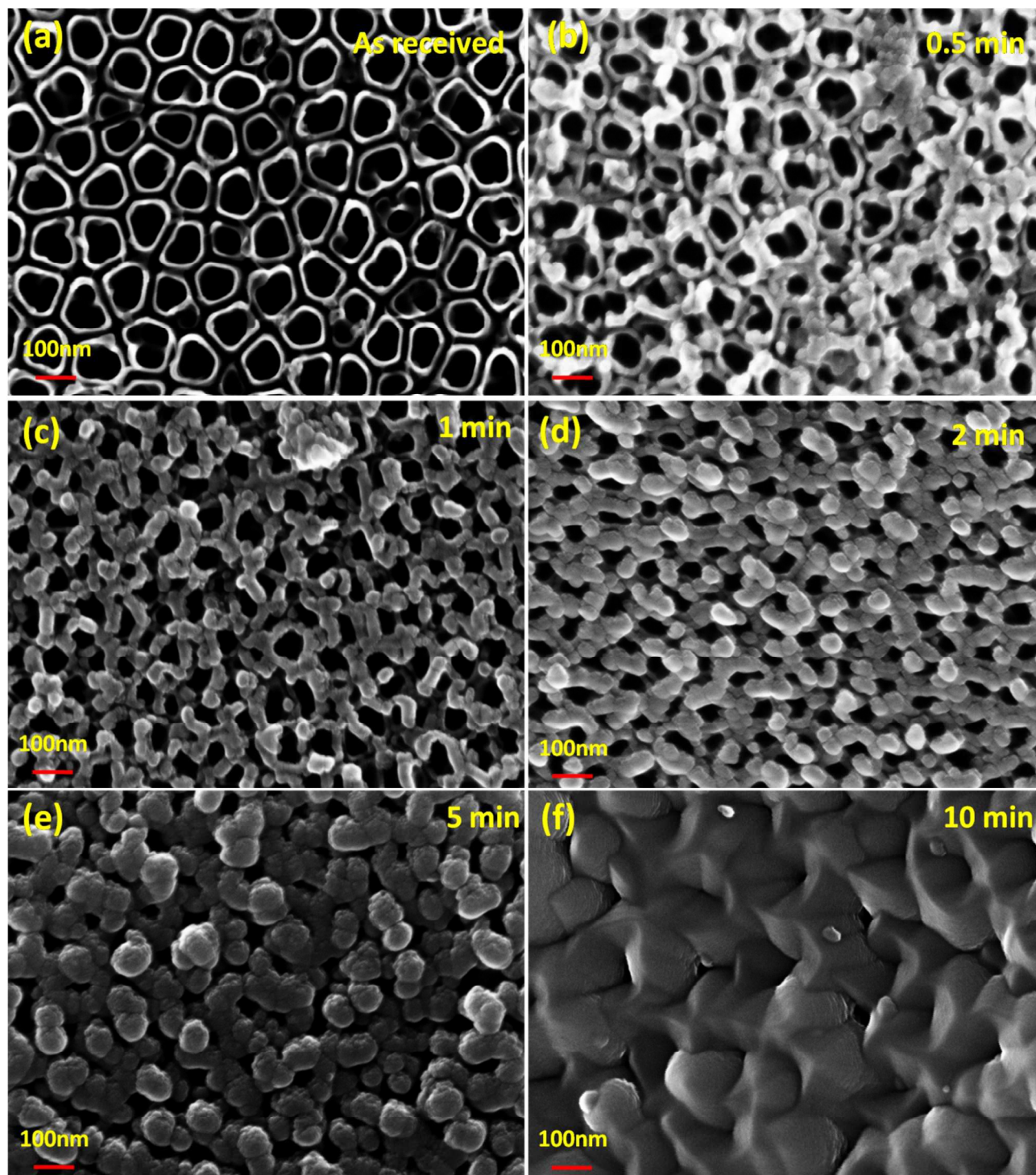


**Fig. 1** FESEM images of TNT (a) and ta-C filled TNT samples at (b) 0.5 min, (c) 1 min, (d) 2 min, (e) 5 min and (f) 10 min.

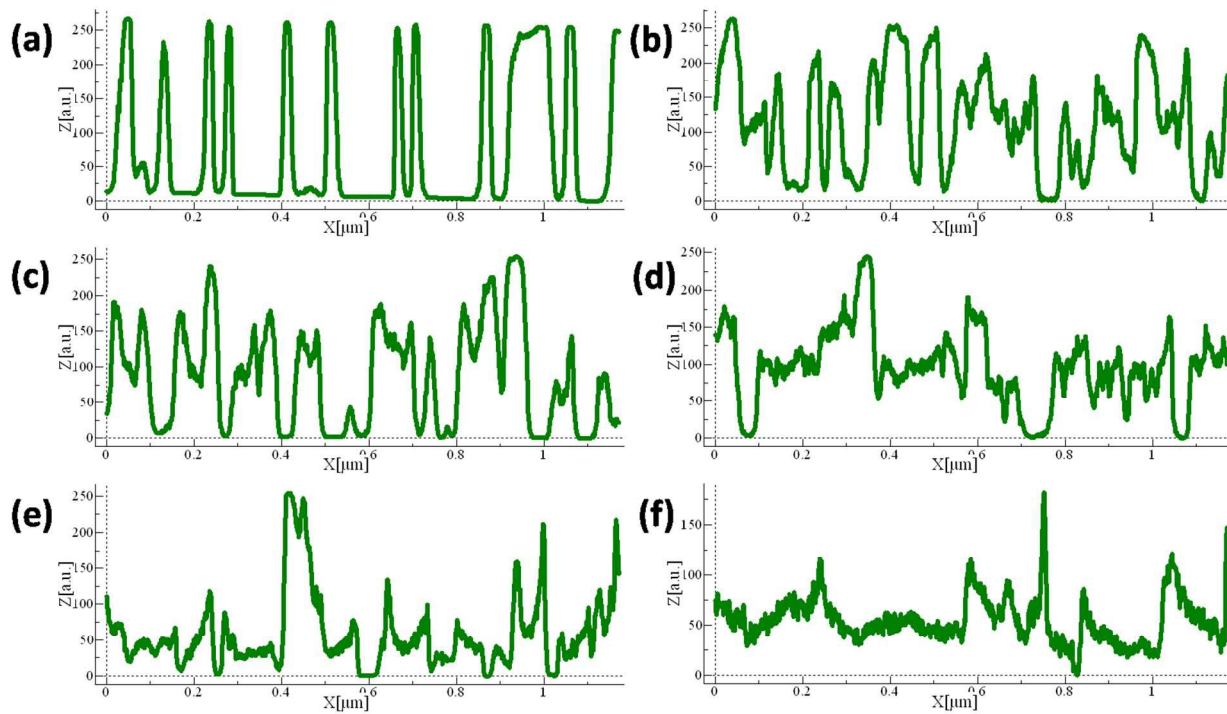


**Fig. 2** 2D line profiles obtained from FESEM images (a) TNT and ta-C filled TNT samples at (b) 0.5 min, (c) 1 min, (d) 2 min, (e) 5 min and (f) 10 min.

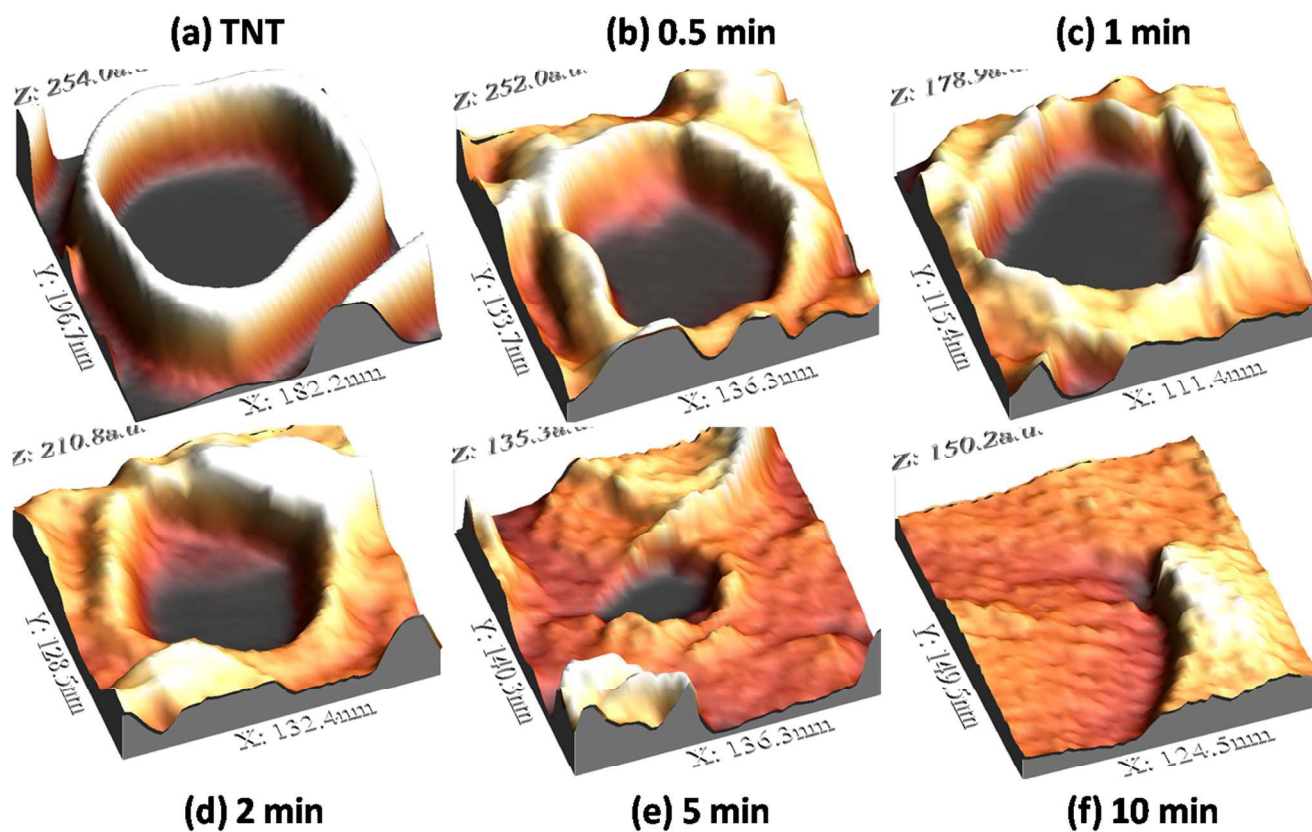


**Fig. 3** 3D images obtained from FESEM images for single nanotube (a) TNT and ta-C filled TNT samples at (b) 0.5 min, (c) 1 min, (d) 2 min, (e) 5 min and (f) 10 min.

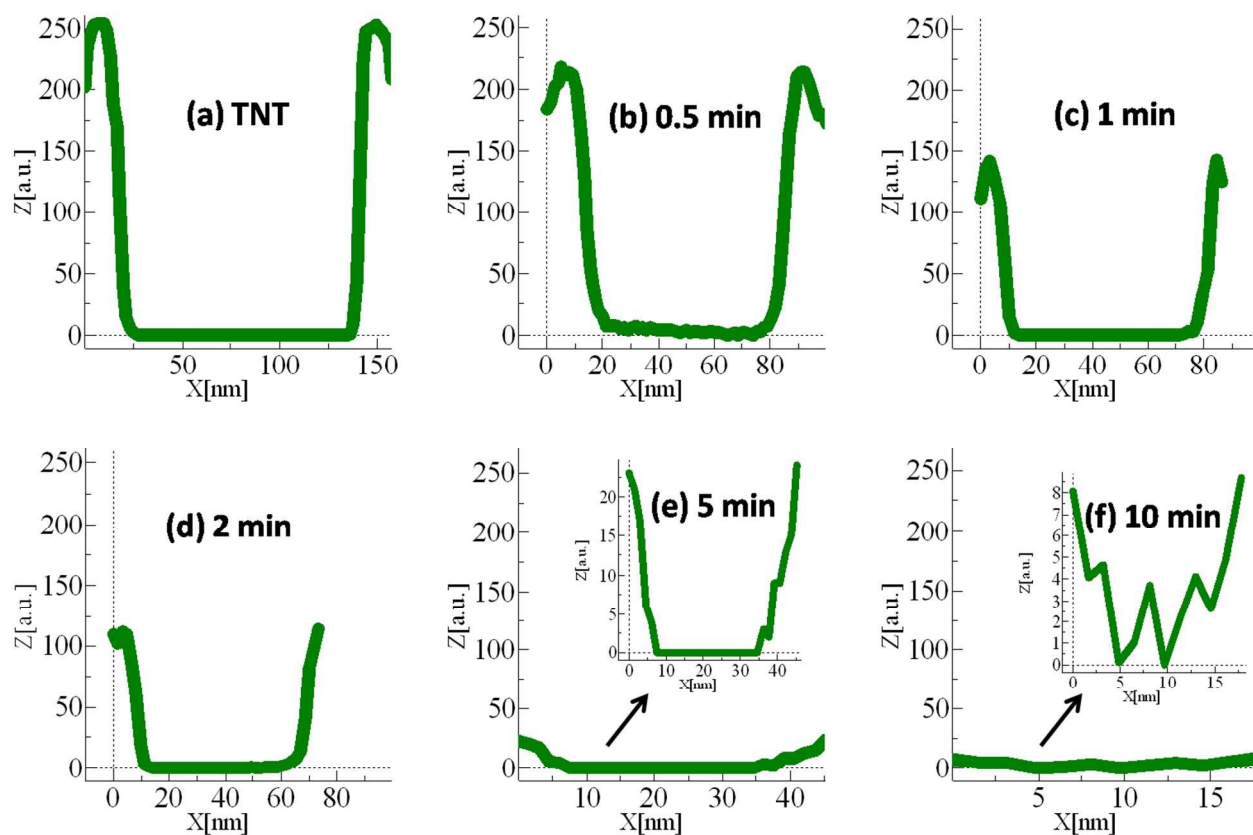


**Fig. 4** 2D profiles obtained from FESEM images for single nanotube (a) TNT and ta-C filled TNT samples at (b) 0.5 min, (c) 1 min, (d) 2 min, (e) 5 min and (f) 10 min.

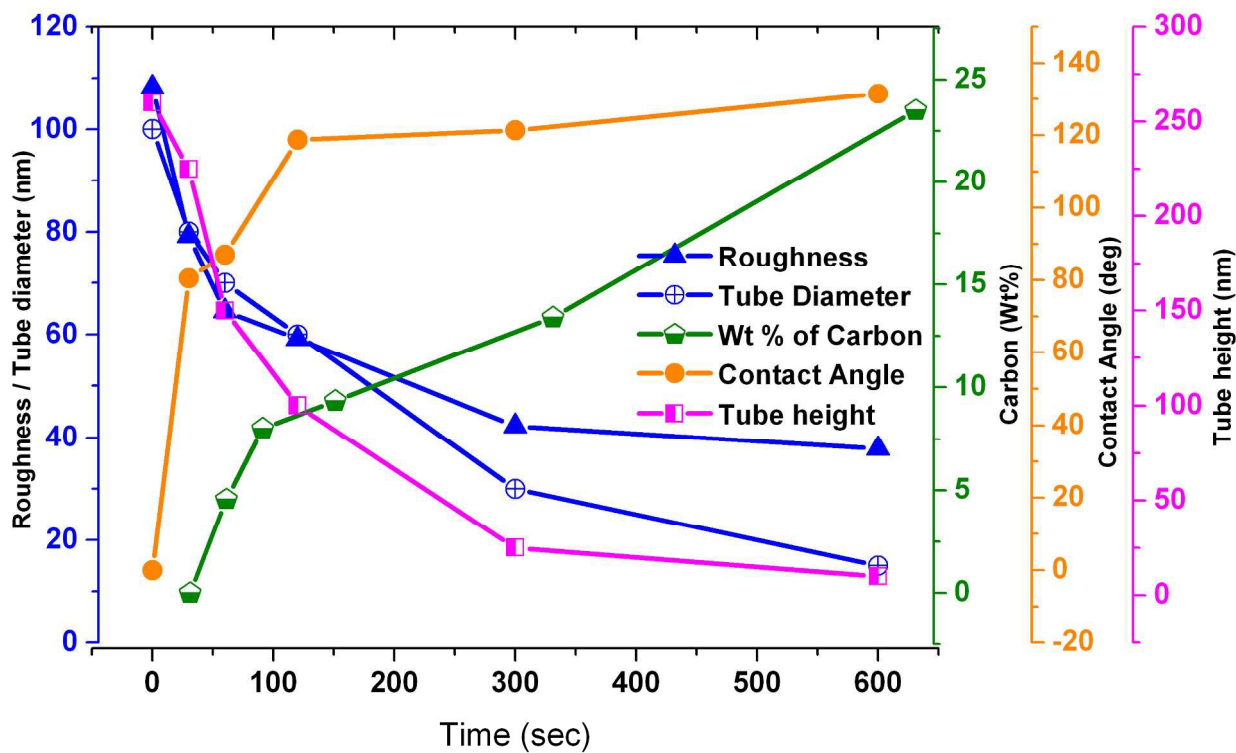


**Fig. 5** Roughness (RMS), nanotube diameter (nm) (Left) and carbon (wt %), contact angle (deg), tube height (nm) (Right) obtained from ta-C filled TNT samples at different filling time (0.5, 1, 2, 5 and 10 min).

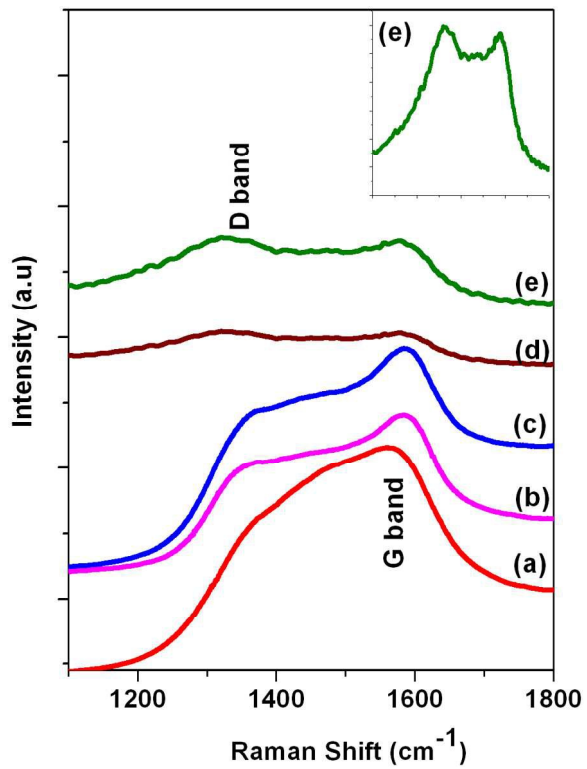


**Fig. 6** Raman spectra for ta-C filled TNT at (a) 0.5 min, (b) 1 min, (c) 2 min, (d) 5 min and (e) 10 min (inset at 10 min).

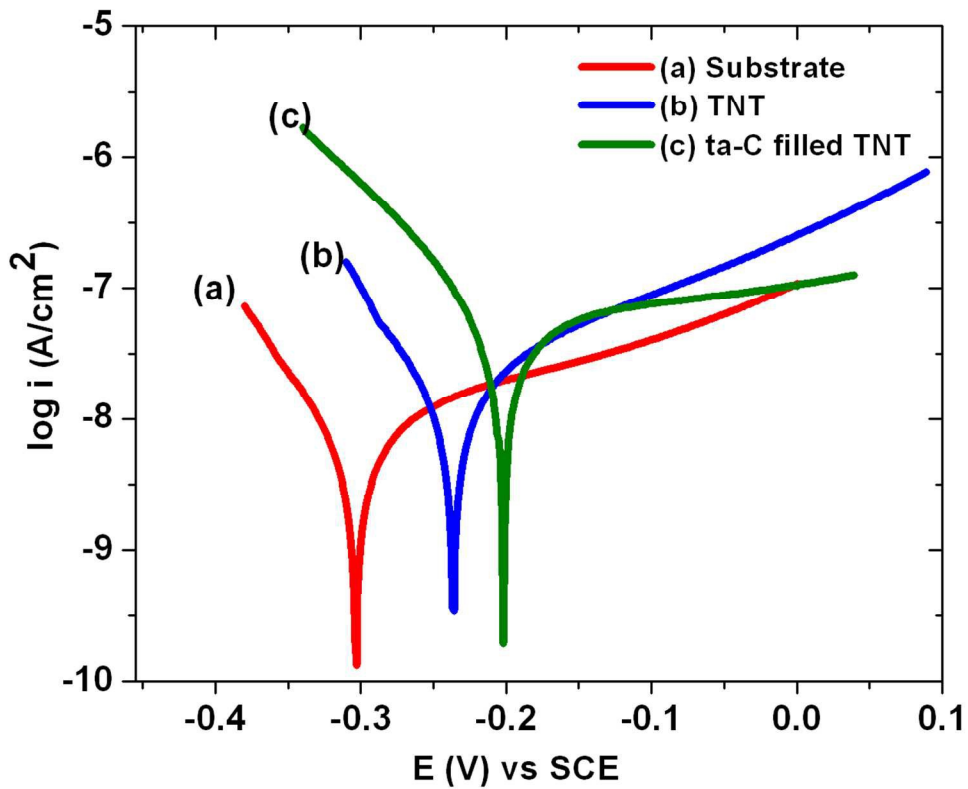


**Fig. 7** Potentiodynamic polarization curves for (a) Ti-6Al-7Nb substrate (b) TNT and (c) ta-C filled TNT samples.

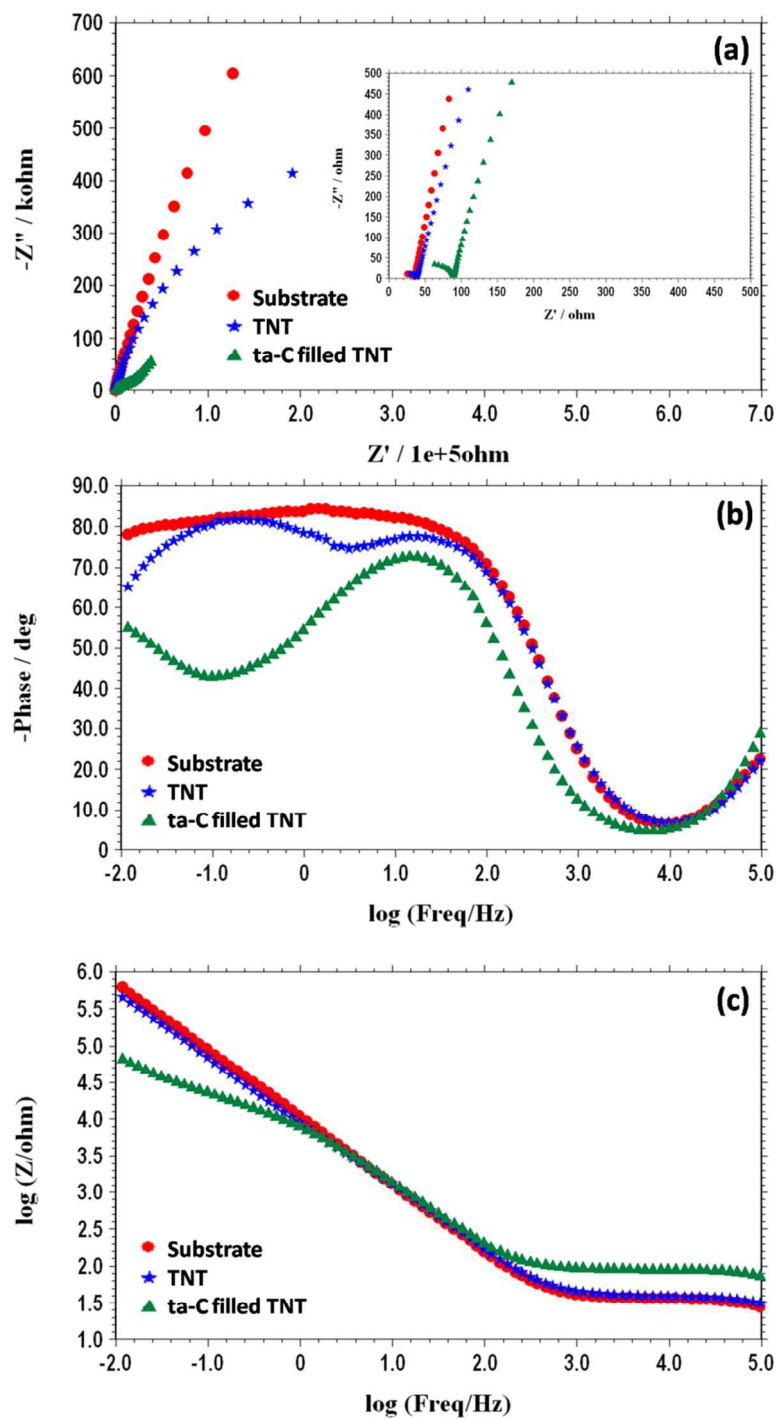


**Fig. 8** (a) Nyquist plot, Bode plots (b) phase and (c) magnitude for substrate, TNT and ta-C filled TNT samples

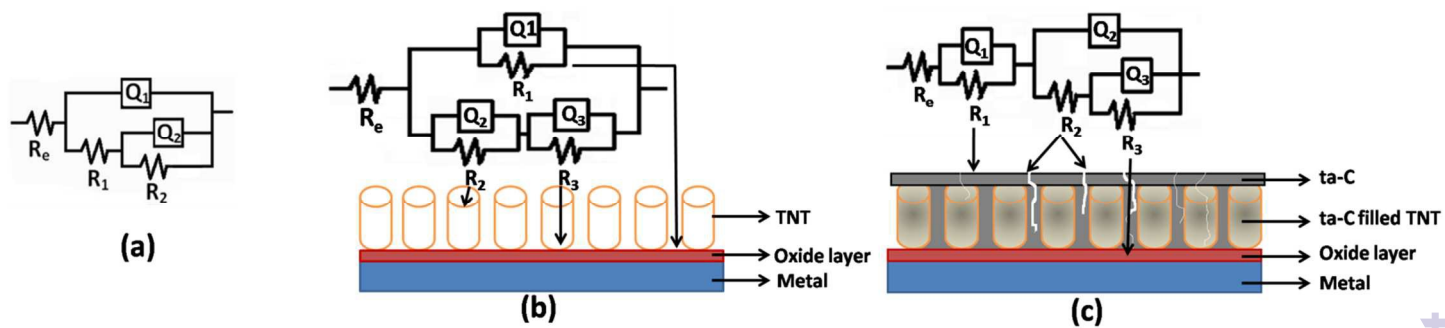


**Fig.9** Equivalent circuit (EC) diagram with schematic representation used for fitting EIS data of (a) substrate, (b) TNT (c) ta-C filled TNT samples.